Materials Science & Engineering A 673 (2016) 467–475

Contents lists available at ScienceDirect

Materials Science & Engineering A

journal homepage: www.elsevier.com/locate/msea

Effects of tempering mode on the structural changes of martensite

D.C. Saha [a,*], E. Biro [b], A.P. Gerlich [a], Y. Zhou [a]

[a] Centre for Advanced Materials Joining, Department of Mechanical & Mechatronics Engineering, University of Waterloo, 200 University Avenue West, Waterloo, Ontario, Canada N2L 3G1

[b] ArcelorMittal Global Research, 1390 Burlington Street East, Hamilton, ON, Canada L8N 3J5

ARTICLE INFO

Article history:
Received 9 June 2016
Received in revised form
20 July 2016
Accepted 22 July 2016
Available online 25 July 2016

Keywords:
Martensite tempering
Transmission electron microscopy
Crystallography
Dislocation density
Nanoindentation
Strength

ABSTRACT

Tempered martensite obtained from four different tempering modes were characterized using transmission electron microscopy, high-angle annular dark field scanning transmission electron microscopy, and nanoindentation techniques. Crystallographic analysis of tempered martensite revealed that ferrite (α) and cementite (θ) obtained via furnace and Gleeble heat treatment obeyed the Isaichev orientation (or close to it) with $[3\bar{1}1]_\theta$ 0.91° from $[1\bar{1}1]_\alpha$ and the $[\bar{1}12]_\alpha \| [001]_\theta$ Bagaryatsky orientation relationship. A strict orientation relationship between ferrite and cementite could not be determined on the tempered structure extracted from the sub-critical heat affected zone of two different laser beam welded samples. Extensive recovery and reduction of boundary regions was identified on the structure tempered slowly, whereas rapidly tempered structures retained a high density of dislocation and less decomposition of the lath structure. The relationship between dislocation density and modified tempering parameter was determined and their contributions on tensile strength were evaluated.

1. Introduction

Tempering of martensitic steels is essential to suppress brittle fracture and ensure a desired combination of strength and ductility. During tempering, the strength of martensitic steel decreases due to ejection of carbon atoms from the carbon supersaturated martensite phase [1]. Martensite tempering involves a series of processes. In the first stage of tempering which occurs between temperature 80–200 °C, the segregation and redistribution of carbon atoms take place into lattice defects such as dislocations, lath boundaries, and prior-γ grain boundaries. In addition, the transitional epsilon-carbides (ε-$Fe_{2.4}C$) also formed in this tempering stage [2–4]. The interlath film like retained austenite decomposes into ferrite (α) and cementite (θ-Fe_3C) in the second stage of tempering (200–300 °C). In the third stage of tempering, segregated carbon and transitional carbides transform into stable carbides such as cementite (Fe_3C), which occurs at higher temperature, in the range of 250–350 °C [4]. At temperatures above 350 °C, the cementite spheroidizes and coarsens [4]. There are numerous factors which influence the martensite tempering process, such as: tempering temperature [5,6], tempering time [5,6], heating rate [7–9], and the steel chemistry [10,11]. Tempering is used in variety of applications, these can be divided broadly into rapid tempering applications and slow (or conventional) tempering applications. In rapid tempering, the tempering occurs on the order of seconds or less. Industrial examples of rapid tempering include: induction heating, laser heat treatment, and tempered heat-affected zone (HAZ) transformations during welding and joining [10–12]. Slow tempering is typically used in furnace post weld heat treatments, and tempering parts made of quench and temper steels. Tempering technique can also affect process costs. For example, induction heating process is cost effective due to the shorter processing time [7,9,13,14]. On the other hand, a conventional tempering cycle is used to obtain a desired homogeneous microstructure with a uniform optimum mechanical property [15]; therefore, the conventional furnace tempering process is suitable for a large-scale component which requires slow cooling to obtain a homogeneous microstructure.

Typical microstructural features such as crystal defect sites (especially with high dislocation densities), lath sizes, and block or packets sizes are influenced by the mode of heating and heating rate. Hernandez et al. [10] studied the consequences of isothermal and nonisothermal tempering process on dual-phase steel. They reported that the nonisothermal process employed using a resistance spot welder produces finer cementite and lesser recovery in the ferrite structure compared to that obtained in a furnace heat treatment (isothermal tempering) process. It has been also reported that steel containing rich alloying elements such as Mn, and Cr has higher resistance to softening compared to a lean Mn and Cr containing steels [11].

The objective of the present study is to examine the tempered structures of 0.24% C containing fully martensitic steel produced

* Corresponding author.
E-mail address: dcsaha@uwaterloo.ca (D.C. Saha).

http://dx.doi.org/10.1016/j.msea.2016.07.092
0921-5093/

with various tempering modes such as a furnace heat treatment (FHT), Gleeble heat treatment (GHT), diode laser welding (DLW), and fiber laser welding (FLW) via transmission electron microscopy (TEM), high-angle annular dark-field scanning TEM (HAADF-STEM) imaging, and nanoindentation study. Crystallographic analysis using selected area diffraction (SAD) patterns and nanoscale microstructure-properties correlations are evaluated. In addition, the strength contribution from high dislocation densities and precipitation are evaluated for the four tempering conditions considered.

2. Experimental

A 1.20 mm thick 0.24% C containing fully martensitic steel were used; the chemical compositions of the investigated steel is shown in Table 1. In order to obtain various tempered structures, different tempering methods were employed with different heating and cooling rates, temperatures, and times (Fig. 1, and Table 2). To produce a FHT sample, tempering was carried out in a muffle furnace at 500 °C for 1 h; and a GHT sample was obtained by heating the sample at a heating rate, temperature, and time of 100 °C/s, 495 °C, and 1 s, respectively (Fig. 1). Two other samples were prepared from the sub-critical HAZ (Ac_1 isotherm line) of diode and fiber laser welded samples, which are henceforth referred as the DLW, and FLW sample, respectively (Fig. 1). It can be noted that the thermal profiles presented in Fig. 1 were measured (using a thermocouple welded to the sheet surface) directly from the HAZ during diode laser and fiber laser welding. Due to the narrow HAZ width (about 400 μm) of FLW, it was not possible to record the temperature close to the Ac_1 isotherm line; however, the heating and cooling sections of the thermal profile was successfully predicted (using a suitable curve fitting method) and extended to Ac_1 line (725 °C) as shown in Fig. 1. The cooling rate in the sub-critical HAZ of the laser welded samples were estimated using the Rosenthal Eq. (1) [16]:

$$\frac{\partial \Theta}{\partial t} = -\frac{2\pi k_s^2}{\alpha}\left(\frac{\upsilon \Delta x}{Q}\right)^2 (\Theta - \Theta_0)^3 \quad (1)$$

where $\partial\Theta/\partial t$ is the cooling rate, k_s is the thermal conductivity of the steel (30 W/m/K), α is the thermal diffusivity of the steel (5.613×10^{-6} m^2/s), υ is the welding speed (m/s), Δx is the sheet thickness (mm), Q is the power input (J/mm^2), Θ, and Θ_0 are temperature (K) of the sub-critical HAZ (998 K) and the ambient temperature (298 K), respectively [17]. The parameters used to temper the samples such as heating rates, cooling rates, temperature, and time are presented in Table 2. In this work, the FHT and DLW processes are categorized as slow tempering modes, and the FLW and GHT are regarded as fast tempering modes due to the differences in heat input, and heating rates.

The microstructure of the tempered structure of the samples were analyzed using a field-emission scanning electron microscope (FE-SEM, Model: Zeiss Leo 1550), and TEM. The particle sizes were measured using an image analysis software (imageJ) from several high-resolution FE-SEM micrographs with a magnification of 100,000 ×; more than 1000 particles were measured for each condition. The carbide sizes presented here are the equivalent circular diameter of the particles with the equivalent area. TEM

Table 1
Nominal composition of the martensitic steel used in this investigation.

C	Mn	P	S	Si	Cr	Mo	Ti
0.24	0.4	0.01	0.01	0.20	< 0.1	< 0.1	0.04

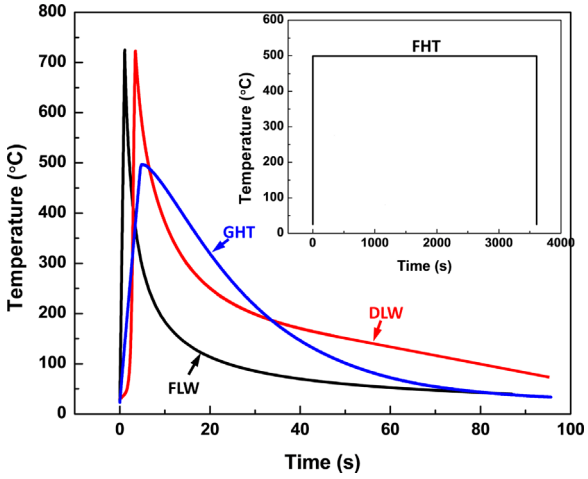

Fig. 1. Thermal cycles imposed on martensitic steels during tempering using a Gleeble heat treatment (GHT), fiber (FLW), diode laser welder (DLW), and furnace heat treatment (FHT).

samples were prepared using twin-jet electropolishing of the 3 mm disks punched from the foils of < 50 μm thickness. Microstructure was analyzed using a JEOL 2010F (Japan Electron Optics Ltd., Tokyo, Japan) electron microscope operated at 200 kV.

Vickers microhardness measurements were carried out using a load of 1 kg with 15 s dwell time; the microhardness value presented here is the average value of 12 individual indents (the tolerance limit represents 95% confidence interval) separated with a spacing of 200 μm. To estimate nanoscale properties of the tempered structures, same Vickers microhardness indented samples were used for the nanoindentation; the study was performed using a Hysitron Triboindenter TI-900 equipped with a scanning probe microscope in a load control condition with a loading rate of 500 μN s^{-1} up to a maximum load of 5000 μN. 12 nano indents (3 × 4 matrix) were made in a 50 μm × 50 μm area with a spacing of about 10 μm between indents.

3. Results and discussion

3.1. As-received martensitic microstructure

Fig. 2 shows the microstructure of as-received material which contains fully autotempered [18] typical lath-like martensite with an estimated prior-γ grain size (measured using a linear intercept method [19]) of about 6.3 ± 0.72 μm (marked with arrows in Fig. 2 (a)). Each prior-γ grain is divided into four packets as outlined with dotted lines in Fig. 2(a). Two kinds of laths were developed during martensitic transformation due to the differences in transformation sequences and temperatures [20]. The coarse laths were formed at the beginning of the martensite formation with relatively high temperature and exhibited reasonably low dislocation density due to greater recovery of dislocations throughout the extended period of transformation [20,21]. On the other hand, thin martensite laths formed at a later stage of martensite transformation which maintained a high dislocation density (Fig. 2(b)). The intralath carbides associated with the autotempered martensite are also delineated in Fig. 2(a). It was observed that the autotempered carbide likely to be precipitated on the coarse martensite laths (thickness: > 500 nm) whereas thin laths with an approximate width of 200 nm were free of autotempered carbides (Fig. 2(b)). TEM micrograph of lath martensite (Fig. 2(b)) indicated different contrast of martensite variants (bright and dark) under certain incident directions of the electron beam. SAD patterns taken from the martensite laths were indexed by following the